Nanoscale Res Lett (2010) 5:882–888
DOI 10.1007/s11671-010-9579-0

NANO EXPRESS

One-Step Synthesis of Monodisperse In-Doped ZnO Nanocrystals

Qing Ling Wang · Ye Feng Yang · Hai Ping He · Dong Dong Chen · Zhi Zhen Ye · Yi Zheng Jin

Received: 23 November 2009 / Accepted: 15 March 2010 / Published online: 31 March 2010

Abstract A method for the synthesis of high quality indium-doped zinc oxide (In-doped ZnO) nanocrystals was developed using a one-step ester elimination reaction based on alcoholysis of metal carboxylate salts. The resulting nearly monodisperse nanocrystals are well-crystallized with typically crystal structure identical to that of wurtzite type of ZnO. Structural, optical, and elemental analyses on the products indicate the incorporation of indium into the host ZnO lattices. The individual nanocrystals with cubic structures were observed in the 5% In–ZnO reaction, due to the relatively high reactivity of indium precursors. Our study would provide further insights for the growth of doped oxide nanocrystals, and deepen the understanding of doping process in colloidal nanocrystal syntheses.

Keywords ZnO · Nanocrystal · Doping · Indium · Monodisperse

Introduction

Transparent conductive oxides (TCOs) are impurity doped metal oxides, such as indium oxide (In_2O_3), zinc oxide (ZnO), and tin oxide (SnO_2), which exhibit excellent properties of controllable low resistivity and high transparency in the visible region [1]. TCOs, generally fabricated as polycrystalline or amorphous thin films, are employed as transparent electrodes in a wide variety of optoelectronic devices, e.g., flat panel displays, light emitting diodes, and photovoltaics [2–4]. Currently, the TCO thin films are deposited by sputtering, thermal deposition, chemical vapor deposition, or other gas phase deposition approaches, which generally require high temperature processing [5, 6]. Nevertheless, high temperature treatments are disadvantageous to be applied on flexible or heat-sensitive substrates [7]. The development of TCO nanocrystals, together with printing techniques, may address the problem and lead to low cost printable transparent electrodes.

Recently, research into the production of TCO nanocrystals, particularly indium-doped tin oxide (ITO) nanocrystals, has steadily increased over the last few years [7–10]. For example, ITO nanoparticles were achieved by an approach comprising microwave-assisted synthesis in ionic liquids [8]. Park et al. prepared colloidal ITO nanoparticles by thermal decomposition of tin and indium precursors in oleylamine [9]. In another study, non-agglomerated ITO nanoparticles were obtained via a combination of nucleophilic attack and condensation–hydrolysis cascade reactions [7]. However, the synthesis of TCO nanocrystals, which corresponds to the growth of doped oxide nanocrystals, still faces significant challenges. A successful synthetic strategy to generate TCO nanocrystals with high crystallinity, narrow size distribution, and homogeneous composition is yet to be achieved. This is due to lack of detailed understanding on the formation of doped nanocrystals, although attempts have been reported in literature. For instance, "self purification", a thermodynamical concept, was invoked to explain the low doping concentration in the case of Mn-doped CdSe nanocrystals [11]. In contrast, Erwin et al. show that for the Mn-doped II–VI nanocrystals doping is controlled by impurity adsorption on the nanocrystal surfaces and the doping

Q. L. Wang · Y. F. Yang · H. P. He · D. D. Chen · Z. Z. Ye · Y. Z. Jin (✉)
State Key Laboratory of Silicon Materials, Department of Materials Science and Engineering, Zhejiang University, Hangzhou 310027, People's Republic of China
e-mail: yizhengjin@zju.edu.cn

efficiency is mainly determined by three factors: surface morphology, nanocrystal shapes, and surfactants in the growth solution [12]. In a recent publication, Chen et al. suggest that the nanocrystal doping processes are strongly temperature-dependent [13]. Further research is essential to uncover the critical factors that govern the growth of doped nanocrystals.

In this article, we describe a simple and facile approach to the generation of In-doped ZnO nanocrystals. We choose to study the In-doped ZnO nanocrystal system because In-doped ZnO thin films have been well-studied, demonstrating superior optoelectronic properties as TCO thin films. In addition, both zinc oxide and indium oxide nanocrystals are readily synthesized by a one-step ester elimination reaction based on alcoholysis of metal carboxylate salts [14, 15]. The reactions can be monitored by Fourier transform infrared spectroscopy (FTIR) and UV–Visible absorption spectra (UV–Vis), making them ideal for investigating the processes. The resulting nanocrystals from the reactions have been characterized by transmission electron microscopy (TEM), high-resolution transmission electron microscopy (HRTEM), energy-dispersive spectroscopy (EDS), inductively coupled plasma atomic emission spectrometer (ICP-AES), X-ray diffraction (XRD), and UV–Vis.

Experimental

Indium acetate ($In(Ac)_3$) and stearic acid (SA) was purchased from Aldrich. Zinc stearate ($Zn(St)_2$) and 1-Octadecanol (ODA) was purchased from Alfa Aesar. 1-Octadecene (ODE, tech 90%) was purchased from Acros. All chemicals were used without further purification.

Indium stearate, which was used as indium precursor in the ester elimination reactions, was prepared as follows [15]. $In(Ac)_3$ (20 mmol) was mixed with SA (80 mmol) and heated to 140 °C under an argon atmosphere. The mixture was heated for 5 h, and then the product was isolated by addition of acetone. The resulting precipitate was filtered, vacuum-dried, and again treated with SA (80 mmol) to ensure complete conversion of acetate to stearate. The final product ($In(St)_3$) was washed several times with acetone to remove excess SA.

Four typical reactions, namely pure ZnO reaction (starting with 1 mmol of $Zn(St)_2$), 2% In–ZnO reaction (starting with 0.02 mmol of $In(St)_3$ and 0.98 mmol of $Zn(St)_2$), 5% In–ZnO reaction (starting with 0.05 mmol of $In(St)_3$ and 0.95 mmol of $Zn(St)_2$), and In_2O_3 reaction (starting with 1 mmol of $In(St)_3$), were studied in this work. In a typical procedure, the metal carboxylate salts and 20 g of 1-octadecene (ODE) were loaded into a three-necked flask. The flask was purged with argon several times, and degassed under vacuum at 120 °C for 20 min with vigorous magnetic stirring. The entire reaction system became a clear solution. Then the solution was heated to 290 °C. 1-Octadecanol (5 mmol) dissolved in 5 g of ODE at 150 °C was quickly injected into the reaction solution. The reaction temperature was set at 290 °C throughout the entire synthesis. After 20 min, the flask was cooled to 50 °C. 50 mL of ethyl acetate were used to precipitate nanocrystals, and the nanocrystals were collected by centrifugation. The nanocrystals were then dispersed in toluene, and any insoluble residue was removed by centrifugation. In-doped ZnO nanocrystals were precipitated by isopropyl alcohol and collected by centrifugation.

Transmission electron microscopy (TEM) and high-resolution TEM images were taken on a JEOL JEM 1230 microscope operated at 80 kV and TECNAI G2 F20 transmission electron microscope at 200 kV equipped with an X-ray energy-dispersive spectroscopy (EDS) system. Specimens were prepared by depositing a drop of $CHCl_3$ solution containing the purified nanocrystals or the aliquots taken during the course of the reaction onto holey carbon-coated Cu grids. X-ray diffraction patterns were obtained on a Bede D1 system operating at 20 kV and 30 mA, using a Cu Kα line ($\lambda = 1.5418$ Å). FTIR spectra were obtained on a Bruker Vector 22 spectrophotometer. The samples were prepared by directly spotting hot aliquots of a reaction mixture onto a KBr crystal. The C=C group peak at 1,641 cm^{-1} was chosen as the reference. IRIS Intrepid II XSP inductively coupled plasma atomic emission spectrometer (ICP-AES) were used for elemental analysis of doped nanocrystals. The optical properties of the colloidal In-doped ZnO nanocrystal solution were analyzed using UNICO UV 2102 ultraviolet–visible spectrophotometer.

Results and Discussion

The introduction of the indium-dopant precursor to the reagents dramatically affects the size of the resulting nanocrystals (Fig. 1). Pure ZnO nanocrystals have an average diameter of 16.1 ± 1.8 nm. The 2% In–ZnO reaction and the 5% In–ZnO reaction yield nanocrystals with sizes of 10.2 ± 0.8 nm and 9.9 ± 0.5 nm, respectively, suggesting that a relatively narrow size distribution. The reduction in the nanocrystal size implies that the indium species play an important role in the growth of the host nanocrystals. The growth rate of nanocrystals is significantly restrained by the adsorption of indium ions during the course of the reaction. Such a size reduction of doped nanocrystals has also been observed in other doped nanocrystal systems. For instance, in the Mn-doped indium oxide system, the dopant ions inhibit the growth of the nanocrystals and stabilize metastable hexagonal type of

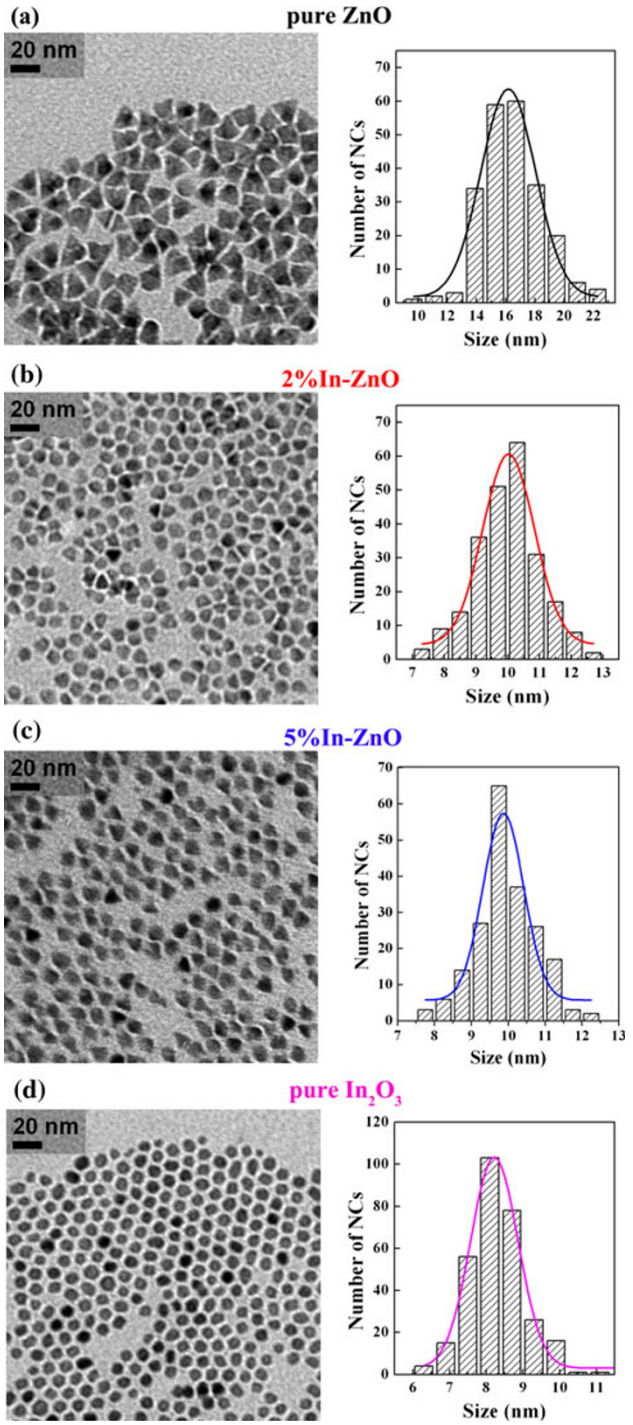

Fig. 1 TEM images (*left*) and size distribution histograms (*right*) of the nanocrystals from (**a**) the pure ZnO reaction, (**b**) the 2% In–ZnO reaction, (**c**) the 5% In–ZnO reaction, and (**d**) the pure In_2O_3 reaction. The curves in histograms are the corresponding Gaussian fits

In_2O_3 nanocrystals with smaller dimensions [16]. For the Eu-doped ZnO nanocrystals, a sequential decrease of the crystallite size with the increasing Eu content was observed [17].

High-resolution transmission electron microscopy (HRTEM) observations reveal the high crystalline nature of the nanocrystals produced by our method. As shown in Fig. 2a–c, the nanocrystals exhibit well defined lattice fringes. The crystal structure of the nanocrystals matches that of wurtzite type of ZnO, indicating that the indium atoms may incorporate into the host lattices and form well-crystallized doped nanocrystals. By carefully checking 162 HRTEM images with clear lattice fringes of nanocrystals from one batch of the 5% In–ZnO reaction, two nanocrystals have cubic crystal structure, identical to that of corundum type of In_2O_3. HRTEM analyses on 155 nanocrystals from another batch of the 5% In–ZnO reaction show that one nanocrystal has cubic crystal structure and all the other nanocrystals possess hexagonal crystal structure corresponding to that of wurtzite type of ZnO. The formation of nanocrystals with the crystal structure identical to that of corundum type of In_2O_3, either pure indium oxide nanocrystals or zinc-doped indium oxide nanocrystals, shall be discussed later in the text. The EDS measurements indicate the presence of indium in the nanocrystals (Fig. 2e). This agrees well with the ICP-AES results that In:(Zn + In) molar ratio is 2.2 and 4.6% for the products from the 2% In–ZnO reaction and the 5% In–ZnO reaction, respectively.

The XRD profiles of the nanocrystals from the pure ZnO reaction, the 2% In–ZnO reaction and the 5% In–ZnO reaction (Fig. 3a) match well with that of bulk wurtzite type of ZnO (hexagonal structure; JCPDS: 36-1451), consistent with the HRTEM results. No additional peaks can be distinguished in the XRD pattern of the In-doped ZnO nanocrystals, excluding the existence of large quantity of nanocrystals with cubic structures. It is noteworthy that the reflections of corundum type of indium oxide are absent even when the reaction starts with 0.2 mmol of $In(St)_3$ and 0.8 mmol of $Zn(St)_2$ (data not shown). For comparison, in the case of Eu-doped ZnO nanocrystals, the diffraction peaks from cubic Eu_2O_3 are evident for the as-synthesized ZnO:10%Eu nanocrystals [17]. By carefully analyzing the XRD data, the full width at half maximum (FWHM) of (100) peak for the products from the pure ZnO reaction, the 2% In–ZnO reaction and the 5% In–ZnO reaction are 0.9°,1.4°, and 1.5°, respectively. According to the Scherrer equation, the larger the FWHM is, the smaller the mean size of the nanocrystals is. Therefore, the size of the nanocrystals from the 2% In–ZnO reaction and the 5% In–ZnO reaction shall be smaller than that of the nanocrystals from the pure ZnO reaction, which agrees with the TEM observations.

The UV–Vis absorption spectra provide more information related to the doping of the nanocrystals. Fitting the data to the sigmoidal formula gives an effective band gap of 3.35, 3.43, and 3.46 eV for the nanocrystals from the

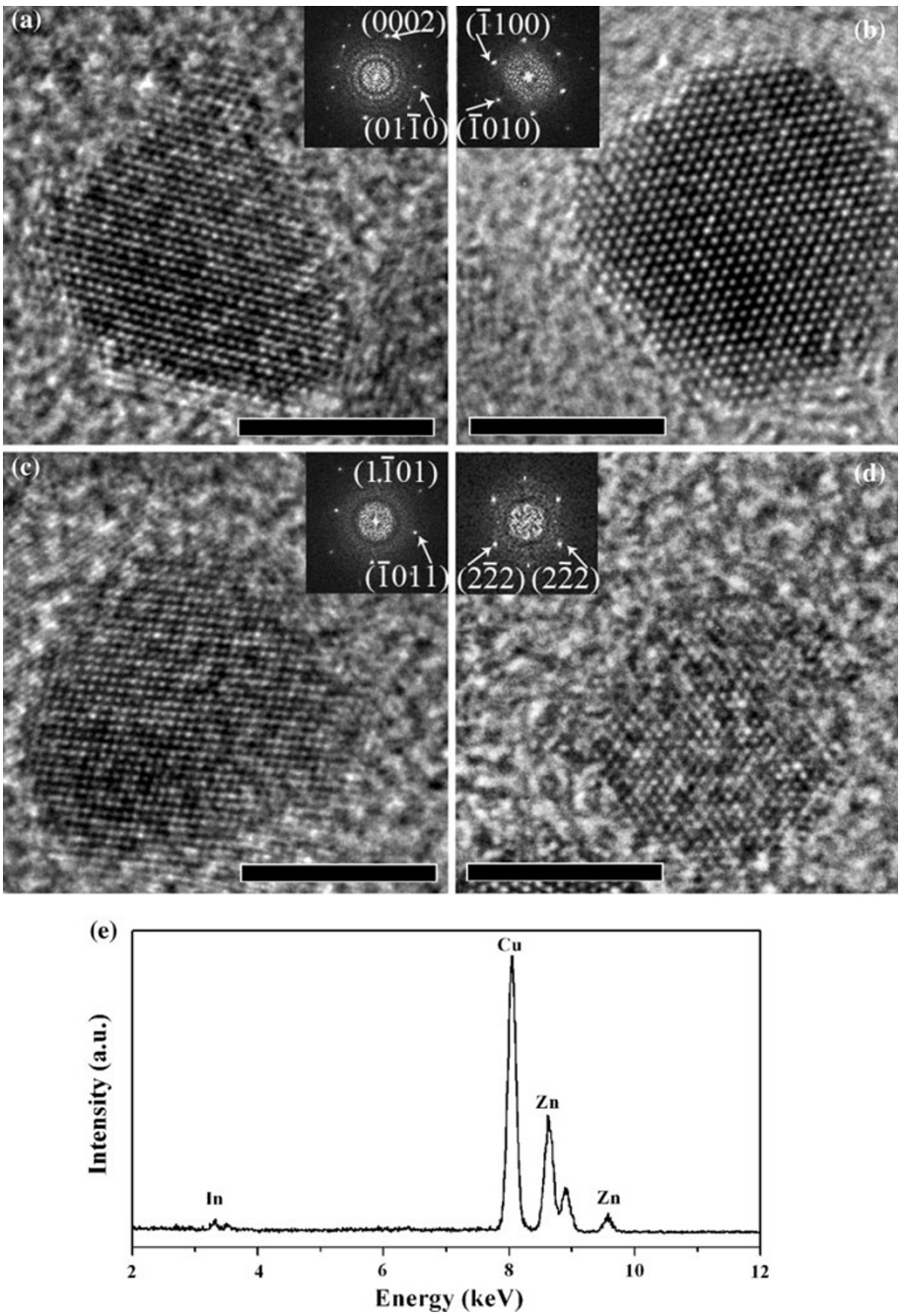

Fig. 2 **a–d** Typical HRTEM images of the nanocrystals from the 5% In-doped nanocrystals. *Insets* are the corresponding FFT patterns. Scale bars are 5 nm. **e** A typical EDS spectrum of the products of the 5% In-doped nanocrystals

pure ZnO reaction, the 2% In–ZnO reaction and the 5% In–ZnO reaction, respectively [18]. The average diameter of the undoped ZnO nanoparticles is *ca.* 16 nm. Thus, the obtained band gap agrees well with the reported bulk value (3.37 eV) at room temperature. While the average diameter of the In-doped nanoparticles is *ca.* 10 nm, about 5–6 times of the exciton Bohr radius of ZnO (1.8 nm), suggesting a likely presence of moderate quantum confinement effect (QCE) [19]. Theoretical calculations predict a blueshift of ~45 meV for ZnO nanoparticles with diameters of *ca.* 10 nm [20]. Therefore, the observed blue-shift shall be due to both QCE and the Burstein–Moss effect associated with heavy doping. Accordingly, the contribution of indium doping to the blueshift of the optical band gap is deduced as ~35 and ~65 meV for the nanocrystals from the 2% In–ZnO reaction and the 5% In–ZnO reaction, respectively. Such a value is smaller than that expected if we assume all the indium ions are on the substitutional sites. In other words, part of the dopant atoms may resident on the surface of nanocrystals, or congregate as nanocrystals with cubic crystal structures which are found in the products from the 5% In–ZnO reactions.

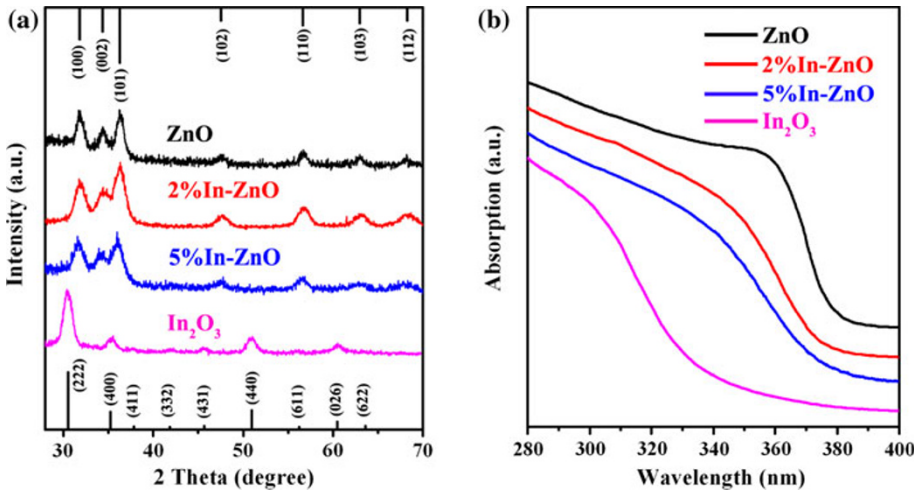

Fig. 3 **a** XRD patterns of the products from the pure ZnO reaction, the 2% In–ZnO reaction, the 5% In–ZnO reaction, and the pure In_2O_3 reaction. The black lines are the patterns of bulk *h*-ZnO and *c*-In_2O_3 with major reflections assigned. **b** UV–Vis spectra of the nanocrystals from the pure ZnO reactions, the 2% In-doped ZnO reactions, the 5% In-doped ZnO reactions, and the pure In_2O_3 reactions

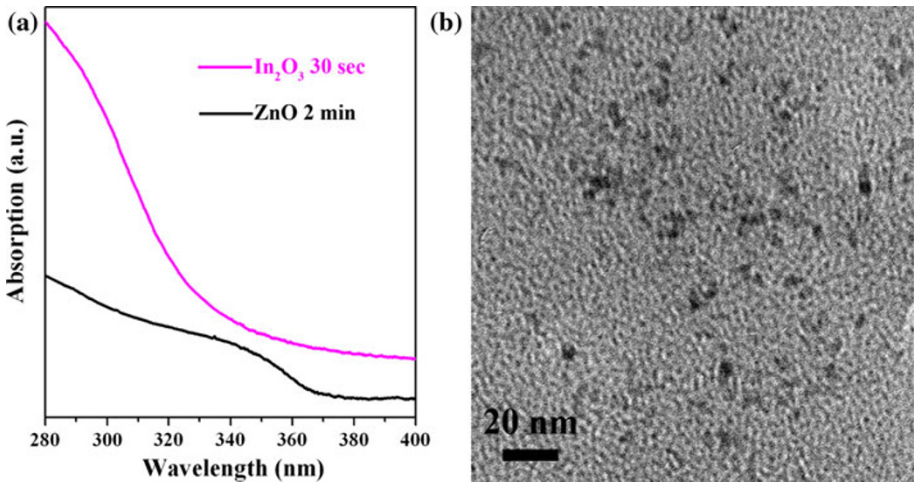

Fig. 4 **a** UV–Vis spectra of the nanocrystals from aliquots taken from the reaction solutions at desirable time. For purification, 1 mL of hexane was added to the aliquots and the unreacted compounds and byproducts were removed by successive methanol extraction until the methanol phase was clear. **b** TEM image of nanocrystals from aliquots taken from solution of the pure In_2O_3 reaction when reaction time is 30 s

We suggest that a higher reactivity of the indium precursor, $In(St)_3$, than that of the zinc precursor, $Zn(St)_2$ accounts for the formation of nanocrystals with cubic structures in the products from the 5% In–ZnO reactions. In the pure In_2O_3 reaction, the formation of In_2O_3 nanocrystals can be detected by UV–Vis spectra only 30 s after the injection of alcohol (Fig. 4a). The initial In_2O_3 nanocrystals were observed by TEM (Fig. 4b). In contrast, the UV–Vis signal of ZnO nanocrystals was detected when the reaction was lasted for 2 min (Fig. 4a). This indicates that zinc carboxylate salts are less reactive than the indium carboxylate salts, which can be confirmed by temporal evolution of FTIR spectra for the pure ZnO reaction and the pure In_2O_3 reaction. The side product of the alcoholysis reactions to generate oxide nanocrystals is ester, which can be detected by FTIR. Therefore, the peak of the C=O stretch (1,740 cm^{-1}) from ester is an ideal indicator to monitor the reactions. As shown in Fig. 5b, for the pure In_2O_3 reaction, the ester peak is evident 30 s after the injection of alcohol, confirming that nucleation of the In_2O_3 nanocrystals occurs in a timescale of <30 s, much faster than that of the ZnO nanocrystals (Fig. 5c). Note that in a study aiming to generate $CuInS_2$ nanocrystals, formation of Cu_xS nanophases was found to be inevitable when indium and copper carboxylates were used as the precursors. Xie et al. demonstrate that this problem can be solved by tuning the relative reactivity of cationic precursors [21]. Therefore, we suspect that by using indium precursors with lower reactivity, pure In-doped ZnO nanocrystals with wurtzite structures may be generated. Further investigations are under way to test this hypothesis.

Conclusions

In-doped ZnO nanocrystals with high crystallinity and relatively narrow size distribution have been synthesized through a one-step reaction based on alcoholysis of metal carboxylate salts. TEM analyses reveal a significant

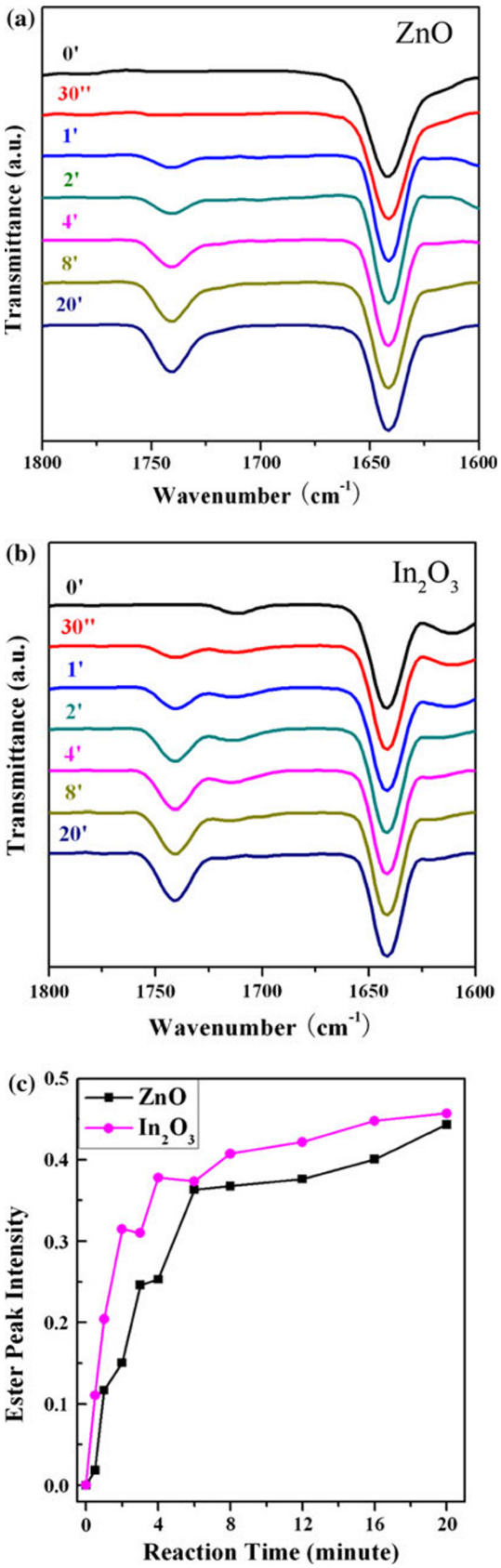

◀**Fig. 5** **a** Temporal evolution of FTIR spectra of the pure ZnO reaction. **b** Temporal evolution of the FTIR spectra of the pure ZnO reaction. All spectra were normalized by the relatively intense C=C vibration band at 1,641 cm^{-1} originating from ODE (the solvent) as the standard. **c** Temporal evolution of the normalized ester peak intensity

reduction in the sizes of the In-doped ZnO nanocrystals compared with that of the undoped ZnO nanocrystals. HRTEM, EDS, ICP-AES, XRD investigations, together with UV–Vis analyses indicate the incorporation of indium into the host ZnO lattices, leading to a blue-shift of the absorption peak. Individual nanocrystals with cubic structures are observed in the products from the 5% In–ZnO reactions, due to the relatively high reactivity of the indium precursor. Our results may provide insights for the growth of doped oxide nanocrystals.

Acknowledgments The study was financially supported by the Zi Jin program of Zhejiang University, Qian Jiang Foundation of Zhejiang Province under Grant No. QJD0702004, and National Natural Science Foundation of China under Grant No. 50802085.

References

1. K. Ellmer, J. Phys. D **33**, R17 (2000)
2. Z. Shen, P.E. Burrows, V. Bulovi, S.R. Forrest, M.E. Thompson, Science **276**, 2009 (1997)
3. V.I. Klimov, S.A. Ivanov, J. Nanda, M. Achermann, I. Bezel, J.A. McGuire, A. Piryatinski, Nature **447**, 441 (2007)
4. J. Herrero, C. Guillen, Thin Solid Films **451–452**, 630 (2004)
5. J. Ni, H. Yan, A. Wang, Y. Yang, C.L. Stern, A.W. Metz, S. Jin, L. Wang, T.J. Marks, J.R. Ireland, C.R. Kannewurf, J. Am. Chem. Soc. **127**, 5613 (2005)
6. P. Canhola, N. Martins, L. Raniero, S. Pereira, E. Fortunato, I. Ferreira, R. Martins, Thin Solid Films **487**, 271 (2005)
7. A.G. Richard Jr., J.C. Charles, G.C. Cantwell, A.G. Rosario, J.S. Christopher, Adv. Mater. **20**, 4163 (2008)
8. G. Bühler, D. Thölmann, C. Feldmann, Adv. Mater. **19**, 2224 (2007)
9. S. Choi, K.M. Nam, B.K. Park, W.S. Seo, J.T. Park, Chem. Mater. **20**, 2609 (2008)
10. J. Ba, D. Fattakhova Rohlfing, A. Feldhoff, T. Brezesinski, I. Djerdj, M. Wark, M. Niederberger, Chem. Mater. **18**, 2848 (2006)
11. F.V. Mikulec, M. Kuno, M. Bennati, D.A. Hall, R.G. Griffin, M.G. Bawendi, J. Am. Chem. Soc. **122**, 2532 (2000)
12. S.C. Erwin, L. Zu, M.I. Haftel, A.L. Efros, T.A. Kennedy, D.J. Norris, Nature **436**, 91 (2005)
13. D. Chen, R. Viswanatha, G.L. Ong, R. Xie, M. Balasubramanian, X. Peng, J. Am. Chem. Soc. **131**, 9333 (2009)
14. Y. Chen, M. Kim, G. Lian, M.B. Johnson, X. Peng, J. Am. Chem. Soc. **127**, 13331 (2005)

15. A. Narayanaswamy, H. Xu, N. Pradhan, M. Kim, X. Peng, J. Am. Chem. Soc. **128**, 10310 (2006)
16. Y.P. Du, Y.W. Zhang, L.D. Sun, C.H. Yan, J. Phys. Chem. C **112**, 12234 (2008)
17. S.S. Farvid, N. Dave, T. Wang, P.V. Radovanovic, J. Phys. Chem. C **113**, 15928 (2009)
18. R.W. Martin, P.G. Middleton, K.P. O'Donnell, W. Van der Stricht, Appl. Phys. Lett. **74**, 263 (1999)
19. V.A. Fonoberov, A.A. Balandin, Phys. Rev. B **70**, 195410 (2004)
20. R. Viswanatha, S. Sapra, B. Satpati, P.V. Satyam, B.N. Dev, D.D. Sarma, J. Mater. Chem. **14**, 661 (2004)
21. R. Xie, M. Rutherford, X. Peng, J. Am. Chem. Soc. **131**, 5691 (2009)